9.5 **SPATIAL DISTRIBUTIONS OF TORNADIC NEAR-STORM ENVIRONMENTS BY CONVECTIVE MODE**

Richard L. Thompson*, Bryan T. Smith, and Andrew R. Dean
NOAA/NWS/Storm Prediction Center
Norman OK

Patrick T. Marsh
University of Oklahoma

1. INTRODUCTION

The characteristics of near-storm environments have been elucidated by several studies of observed soundings near reported tornadoes (Maddox 1976; Kerr and Darkow 1996), all soundings for multiple severe weather hazards during a complete year (Rasmussen and Blanchard 1998), or long-period samples of soundings associated with severe thunderstorms (Craven and Brooks 2004). Meanwhile, much attention in recent years has focused on convective mode and its influences on severe thunderstorm and tornado events. For example, Trapp et al. (2005) examined tornado events attributed to quasi-linear convective systems (QLCS) across the contiguous United States. Gallus et al. (2008) looked at a range of convective mode categories associated with severe thunderstorms across the Midwestern United States. Later work by Duda and Gallus (2010) examined severe weather events with radar-observed supercells in the Midwestern United States. Grams et al. (2012) combined environmental data with simple convective mode categories to compare tornado and significant severe thunderstorm events across the CONUS.

Specific storm modes, including tornadic and nontornadic supercells, were part of the Thompson et al. (2003; 2007) proximity sounding studies, which also relied on short-term forecast model soundings in close proximity to radar-observed supercells. However, these studies focused on discrete storms only and were somewhat limited by sample size. Building on the strengths of this previous work, Smith et al. (2012; hereafter S12) created a convective mode database for a very large sample of severe thunderstorm and tornado events (22 901 total) over a 9-year period across the contiguous United States (CONUS). Thompson et al. (2012; hereafter T12) combined the S12 convective mode sample with RUC model analysis data archived at the Storm Prediction Center (Schneider and Dean 2008) to compare QLCS and right-moving supercell tornado environments. The large sample of near-storm environmental data allowed for seasonal comparisons of tornado environments by convective mode. Still, the explicit regional variations in near-storm environments were only addressed indirectly. The goal of this work is to utilize the T12 convective mode and environmental sample to develop CONUS-wide spatial distributions of near-storm environmental ingredients by convective mode for tornadoes. Such distributions will allow the development of explicit regional climatology of near-storm environmental ingredients for several specific convective modes and associated tornadoes.

2. DATA AND METHODS

The convective mode database described in S12 served as the basis for this analysis. Tornado reports from 2003-2011 across the CONUS were filtered for the maximum damage rating per hour, on a grid with 40 km horizontal spacing. A radar-derived convective mode was assigned to each event based on level-II data from the closest WSR-88D site. The following convective mode categories were identified: 1) right-moving supercells (RM) and left-moving supercells; 2) QLCS; and 3) disorganized cells or clusters not meeting RM or QLCS criteria. Supercells were identified via manual examination of full volumetric reflectivity and velocity data. Mesocyclone identification relied on the mesocyclone nomograms developed by the Warning Decision Training Branch of the National Weather Service (after Andra 1997), where both cyclonic and anticyclonic circulations extended through at least

* *Corresponding author address*: Richard L. Thompson, NOAA/NWS/NCEP/Storm Prediction Center, 120 David L. Boren Blvd., Norman, OK 73072; email: Richard.Thompson@noaa.gov.

25% of the vertical depth of the storm, for a period of at least 10-15 minutes. Following the general methodology of Trapp et al. (2005), QLCS events were defined as continuous radar reflectivity bands of ≥ 35 dBZ (≥ 100 km in length) in the lowest elevation angle, with a length to width aspect ratio of at least 3 to 1.

Near-storm environmental data also accompanied the S12 sample in T12. The Storm Prediction Center maintains a real-time archive of sounding-derived parameters related to severe thunderstorms and tornadoes (i.e., SPC Mesoanalysis data; Schneider and Dean 2008). The data are derived from the hourly RUC model analyses (Benjamin et al. 2004) on a grid with 40 km horizontal spacing, following the objective analysis procedure outlined in Bothwell et al. (2002). Each grid-hour tornado event was assigned a unique convective mode category, as well as various sounding-derived parameters for the nearest grid point and closest hour prior to the tornado beginning time.

This work focuses on the spatial distributions of the RM tornado-related parameters examined by T12, for tornado events with RM, QLCS, and disorganized storms. Specifically, we narrow our analysis to the Significant Tornado Parameter (STP; Thompson et al. 2003) and its four constituent ingredients: 1) lowest 100 mb mean-layer (ML) CAPE; 2) MLLCL height; 3) 0–6-km bulk wind difference; 4) 0–1-km storm-relative helicity (SRH). The total number of grid-hour events (with accompanying near-storm environment data) was accumulated within each 40 km grid box (Fig. 1). A nine year sample is insufficient to capture the full variability of tornado occurrences by specific convective mode on a 40 km horizontal grid, given the rarity of tornadoes with specific storm types, and the inherent noise in the distribution. To address this concern, we accumulated all tornado events within a 120 km neighborhood centered on each grid point, effectively increasing the sample size and smoothing smaller-scale variability in the distributions. Only neighborhoods containing at least 10 tornado events for each convective mode category were included in the plots. Additionally, data were contoured and smoothed via a kernel density estimate with an effective radius of influence of 100 km, similar to the approaches used by Brooks et al. (1998), Sobash et al. (2011), and Marsh et al. (2012) which used a 120 km radius of influence.

3. RESULTS

As discussed in Section 2, sample size limitations prevented a continuous analysis across the entire contiguous United States for each convective mode category. Some of the variability in the analysis is related to the longer-term climatology of tornadoes [e.g., the lower number of events west of the Rockies and in Maine (see Fig. 1), after Kelly et al. (1978) and Brooks et al. (2003)]. The effects of our neighborhood procedure can be seen in the extension of values off the Gulf of Mexico and Atlantic coasts in Fig. 2, where tornado reports (and related convective modes) were not part of the initial sample.

Moreover, the details of the kernel density plots cannot be taken literally in areas where events were not sampled (i.e., across international borders and coastlines) during 2003-2011. The gradients in the kernel density estimate in these areas show artificially low values in areas with relatively few events, adjacent to areas with higher event frequency. Thus, we present both the gridded values (within 120 km of each 40 km grid box) and the smoothed kernel density contour analyses to complement interpretation of the data and to illustrate aspects of variability in our sample of tornado grid-hour events.

3.1 RM Tornadoes

MLCAPE is typically larger across the Great Plains with tornadic RM [2000-4000 J kg^{-1} for the upper-half (50th to 90th percentiles) of the distribution shown in Figs. 2c-f], with consistently weaker MLCAPE along and east of the Appalachians. MLCAPE values with tornadic RM usually do not exceed 1500 J kg^{-1} east of the Mississippi River. Still, relatively low MLCAPE values (10th percentile values ~500 J kg^{-1}) occur occasionally into the Great Plains region, which confirms that tornadic RM can occur in a wide range of buoyancy across much of the CONUS east of the Rocky Mountains.

MLLCL heights show a general tendency to be higher (i.e., >1500 m AGL) with tornadic RM across the high Plains region from the west Texas and eastern New Mexico border northward across the high Plains. Meanwhile, MLLCL heights are generally lower than 1500 m AGL with the vast majority of tornadic RM across the Mississippi Valley and eastern states (Fig. 3). It is important to note that MLLCL height is considered to be a limiting factor for significant (≥ EF2) tornadoes with

RM (after Markowski et al. 2002; Rasmussen 2003, and Thompson et al. 2003, among others), and that these plots show the percentile ranks for all tornadic RM in the sample (including EF0-EF1 tornadoes).

Not surprisingly, 0–6-km bulk wind difference (BWD) with tornadic RM falls in the range typically associated with supercells (roughly ≥ 35 kt per Thompson et al. 2003), even in the lower end of the distribution (Figs. 4a-b). This measure of deep-layer vertical wind shear tends to be strongest across parts of the Mississippi and Tennessee Valleys, which overlaps a large part of the corridor where significant RM tornadoes are also most common (Smith et al. 2012).

Low-level vertical wind shear, as represented by 0–1-km SRH in Fig. 5, shows a marked tendency to be largest across the lower Mississippi and Tennessee Valley regions, much like the distribution of 0–6-km BWD shown in Fig. 4. Weaker tornadoes make up the majority of the low end of the 0–1-km SRH distribution shown in Figs. 5a-b, where the area centered on Mississippi and Alabama is the only consistent area with SRH values considered sufficient for significant tornadoes. Meanwhile, 0–1-km SRH remains lower than 100 m^2 s^{-2} across much of the Great Plains at the 10th percentile with most of these Plains RM tornadoes being rated as weak (EF0-EF1) in terms of damage.

The STP highlights the apparent compensating effects of buoyancy and vertical shear, where the largest STP values correspond to the overlap of the larger MLCAPE values in the Great Plains with the stronger vertical shear across the Mississippi Valley and southeast states (Fig. 6). In general, the corridor of largest STP at the 90th percentile (Figs. 6c-f) extends from the central Plains to Mississippi and Alabama, which is the same corridor favored for significant RM tornadoes in the spring (see Fig. 14 in S12).

3.2 QLCS Tornadoes

Buoyancy is clearly weaker in QLCS tornado environments compared to tornadic RM environments, based on a comparison of Figs. 2 and 7. The most pronounced differences are across the southeast states where MLCAPE rarely exceeds 1000 J kg^{-1} with QLCS tornadoes, and across the Great Plains where QLCS tornadoes are uncommon. Spatial variability is also larger with MLCAPE in QLCS environments (compared to RM environments), though much of this apparent variability could be due to a noticeably smaller sample size of QLCS tornadoes versus RM tornadoes (1168 vs. 7669, respectively). As discussed in T12, MLCAPE is a reasonable discriminator between tornadic RM and tornadic QLCS environments, especially in the winter across the southeast states when buoyancy is weakest climatologically.

MLLCL heights rarely exceed 1500 m AGL in QLCS tornado environments, especially east of the Great Plains (Fig. 8). The primary difference from RM tornado environments is the lack events across the high Plains, other than the small area of QLCS tornado events with relatively high LCLs across northwest Kansas.

Interestingly, the distribution of 0–6-km BWD with QLCS tornadoes (Fig. 9) is quite similar to that of RM tornadoes (Fig. 4), where the majority of tornado cases with both convective modes fall into the part of the parameter space associated with supercells. Many factors affect convective mode, including the degree and spatial patterns of low-level ascent, and the magnitude and orientation of deep-layer vertical shear vectors relative to surface boundaries that serve to focus thunderstorm initiation (e.g., Dial et al. 2010). Thus, more information than a single shear parameter is needed to help identify convective mode.

Where RM and QLCS tornadoes are relatively common (refer to the Mississippi and Tennessee Valley region in Figs. 5 and 10), 0–1-km SRH values are similar across the two convective modes and well into the range associated with tornadic RM (Rasmussen 2003 and Thompson et al. 2003). The assumed rightward storm motion (Bunkers et al. 2000) in the SRH estimate is not necessarily applicable to linear convective systems. However, SRH does serve as a consistent means of comparing vertical shear environments since the storm motion estimate is based solely on the structure of the wind profile.

Overall, the Significant Tornado Parameter is typically weaker in QLCS environments (Fig. 11), owing largely to weaker buoyancy compared to tornadic RM environments. It is important to note that the STP is designed to highlight significant (≥ EF2 damage) tornadoes, and the majority of the tornadoes included in this analysis (90% of QLCS and 82% of RM) produced only weak (EF0-EF1) damage.

3.3 Tornadoes with Disorganized Storms

As expected, tornadoes with disorganized storms occur in a wide range of buoyancy (Fig. 12), and generally weak low-level wind shear (Fig. 15). However, the distribution of disorganized tornado events is quite noisy. One coherent pattern appears to occur across Florida and the Texas Gulf coast, where moderate buoyancy coincides with low LCL heights (Fig. 13) and weak vertical shear (Figs. 14 and 15), with a majority of the tornadoes likely associated with local sea breeze and outflow boundary interactions in the summer (e.g., Collins et al. 2000). Another consistent area is centered on northeast Colorado, where weak-moderate buoyancy coincides with relatively higher LCL heights and weak SRH, where nonsupercell tornadoes are common (e.g., Wakimoto and Wilson 1989; Brady and Szoke 1989).

Curiously, there are disorganized tornadic storms in environments with 0–6-km BWD into the range associated with RM. A specific example is across the central valley of California (Fig. 14e). The majority of these tornado events occurred during the cool season in association with strong synoptic systems, but minimal buoyancy, as documented by Monteverdi et al. (2003). Given the weak buoyancy and small size of the storms often observed in such regimes, supercell structures may not always be resolvable by the closest WSR-88D sites. In contrast, the separate area of tornado events across southern California includes a mix of cool season and warm season events, hence the larger variability in MLLCL heights across southern California compared to northern California.

One obvious outlier signal exists in the STP distribution across northern Mississippi and western Tennessee (Figs. 16e-f). Here, the 90th percentile of STP exceeds 10, which is the result of three specific tornado grid-hour events (all EF0 with minimal path lengths) from the morning of 5 May 2003. The environment consisted of moderate buoyancy (MLCAPE near 2000 J kg^{-1}), a moist boundary layer with MLLCL heights just above 500 m AGL, and strong vertical wind shear (0–6-km bulk wind differences near 65 kt and 0–1-km SRH greater than 400 m^2 s^{-2}). Despite the aforementioned storm environment, close examination of WSR-88D imagery from this case confirms a lack of organized storm structures in association with the tornado reports.

4. DISCUSSION AND SUMMARY

The spatial distributions of supercell-tornado ingredients show distinct patterns that reflect the geography and synoptic climatology of each region. For example, MLCAPE is clearly greatest across the Plains states in tornadic RM environments, with the largest values often exceeding 3000-4000 J kg^{-1}. By comparison, MLCAPE is typically less than 2000 J kg^{-1} across the southeast states in tornadic RM environments. Still, buoyancy can be large across the southeast states in the more extreme events, such as the 27 April 2011 tornado outbreak across Mississippi and Alabama. MLCAPE for the 27 April outbreak ranged from 2500-3500 J kg^{-1} for all of the Alabama grid-hour events, which is above the 90th percentile for MLCAPE in this area (see Fig. 2).

Likewise, MLLCL heights can vary substantially across the Great Plains in tornadic RM environments. The sample climatology shown in Fig. 3 clearly supports a wide range of LCL environments across the Great Plains, with MLLCL heights spanning a range from 500-2500 m AGL for tornadic RM. Variability is much less across the southeast states where MLLCL heights rarely exceed 1500 m AGL. This lower variability can be explained largely by lesser fluctuations in the magnitude of low-level moisture, with low-level trajectories into the southeast States, ranging from the southwest to the southeast, all emanating from the upstream moisture source region of the Gulf of Mexico (e.g., Thompson et al. 1994). Hence, the warm sectors of synoptic cyclones are often relatively moist across the southeast states, and LCL heights are relatively low. In contrast, low-level trajectories from the south and southeast are typically needed to draw richer moisture into the Great Plains. The presence of the Rocky Mountains and plateau to the west typically contributes to steep midlevel lapse rates over the Great Plains in flow regimes with a westerly midlevel flow component (e.g., Lanicci and Warner 1991a, b, c).

Vertical wind shear on the scale of the 40 km RUC analyses tends to be strong and clearly favorable for tornadic RM in the more extreme events (i.e., the significant tornado events which tend to reside near or above the 90th percentile values in Figs. 4 and 5), across the majority of the United States from the eastern part of the Great Plains to the Atlantic coast. Though measures of vertical wind shear have proven to be among the strongest

discriminators between significantly tornadic and nontornadic RM (e.g., Thompson et al. 2003), parameters such as 0-1-km SRH may not be the best discriminators within a given region. Based on prior analyses and supported by results shown here, buoyancy (and midlevel temperatures lapse rates) may be one of the better discriminators between the more significant RM tornado events and nontornadic RM or QLCS tornadoes across the southeast states. Likewise, low-level moisture (and hence MLLCL) is one of the better discriminators between significantly tornadic RM and nontornadic RM across the Great Plains, where steep midlevel lapse rates and large buoyancy are more common. The tendency for compensating environmental ingredients is reflected in the STP distributions shown in Figs. 6e-f, where extreme STP values are relatively consistent from the mid South to the central Great Plains.

The primary value in the analyses presented herein is the graphical representation of the spatial variation of the various tornado-related environmental parameters. Such plots allow meteorologists to efficiently characterize the near-storm environment with consideration for regional climatology, by convective mode. Use of this information can reduce reliance on anecdotal evidence supporting "extreme" environments, or proximity sounding studies that may be dominated by events from a different region (e.g., Thompson et al. 2003). The analyses presented herein are limited primarily by the the representativeness of our sample of events from 2003-2011, and the degree to which the SPC environmental dataset represents the state of the atmosphere.

REFERENCES

Andra, D. L., Jr., 1997: The origin and evolution of the WSR-88D mesocyclone recognition nomogram. Preprints, *28th Conf. on Radar Meteor.*, Austin, TX, Amer. Meteor. Soc., 364–365.

Benjamin, S. G., and Coauthors, 2004: An hourly assimilation-forecast cycle: The RUC. *Mon. Wea. Rev*., **132**, 495-518.

Bothwell, P. D., J. A. Hart, and R. L. Thompson, 2002: An integrated three-dimensional objective analysis scheme in use at the Storm Prediction Center. Preprints, *21st Conf. on Severe Local Storms*, San Antonio, TX, Amer. Meteor. Soc., J117–J120.

Brady, R. H., and E. J. Szoke, 1989: A case study of nonmesocyclone tornado development in northeast Colorado: similarities to waterspout formation. *Mon. Wea. Rev*., **117**, 843–856.

Brooks, H. E., C. A. Doswell III, and M. P. Kay, 2003: Climatological estimates of local daily tornado probability for the United States. *Wea. Forecasting*, **18**, 626-640.

_____, M. Kay, and J. A. Hart, 1998: Objective limits on forecasting skill for rare events. Preprints, 19th Conf. on Severe Local Storms, Minneapolis MN, Amer. Meteor. Soc., 552–555.

Bunkers, M. J., B. A. Klimowski, J. W. Zeitler, R. L. Thompson, and M. L. Weisman, 2000: Predicting supercell motion using a new hodograph technique. *Wea. Forecasting*, **15**, 61–79.

Collins, W. G., C. H. Paxton, and J. H. Golden, 2000: The 12 July 1995 Pinellas County, Florida, tornado/waterspout. *Wea. Forecasting*, **15**, 122–134.

Craven, J. P., and H. E. Brooks, 2004: Baseline climatology of sounding derived parameters associated with deep moist convection. *Nat. Wea. Digest*, **28**, 13-24.

Dial, G. L., J. P. Racy, and R. L. Thompson, 2010: Short-term convective mode evolution along synoptic boundaries. *Wea. Forecasting*, **25**, 1430-1446.

Duda, J. D., and W. A. Gallus, Jr., 2010: Spring and summer Midwestern severe weather reports in supercells compared to other morphologies. *Wea. Forecasting*, **25**, 190-206.

Gallus, W. A., Jr., N. A. Snook, and E. V. Johnson, 2008: Spring and summer severe weather reports over the Midwest as a function of convective mode: A preliminary study. *Wea. Forecasting*, **23**, 101–113.

Grams, J. S., R. L. Thompson, D. V. Snively, J. A. Prentice, G. M. Hodges, and L. J. Reames, 2012: A climatology and comparison of parameters for significant tornado events in the United States. *Wea. Forecasting*, **27**, 106-123.

Kelly, D. L., J. T. Schaefer, R. P. McNulty, C. A. Doswell III, and R. F. Abbey Jr., 1978: An augmented tornado climatology. *Mon. Wea. Rev*., **106**, 1172-1183.

Kerr, B. W., and G. L. Darkow, 1996: Storm-relative winds and helicity in the tornadic thunderstorm environment. *Wea. Forecasting*, **11**, 489–505.

Lanicci, J. M., and T. T. Warner, 1991a: A synoptic climatology of the elevated mixed-layer inversion over the southern Great Plains in spring. Part I: Structure, dynamics, and seasonal evolution. *Wea. Forecasting*, **6**, 181-197.

_____, and _____, 1991b: A synoptic climatology of the elevated mixed-layer inversion over the southern Great Plains in spring. Part II: The life cycle of the lid. *Wea. Forecasting*, **6**, 198-213.

_____, and _____, 1991c: A synoptic climatology of the elevated mixed-layer inversion over the southern Great Plains in spring. Part III: Relationship to severe-storms climatology. *Wea. Forecasting*, **6**, 214-226.

Maddox, R. A., 1976: An evaluation of tornado proximity wind and stability data. *Mon. Wea. Rev*., **104**, 133–142.

Markowski, P. M., J. M. Straka, and E. N. Rasmussen, 2002: Direct surface thermodynamic observations within the rear-flank downdrafts of nontornadic and tornadic supercells. *Mon. Wea. Rev*., **130**, 1692-1721.

Marsh, P. T., J. S. Kain, V. Lackshmanan, A. J. Clark, N. M. Hitchens, and J. Hardy, 2012: A method for calibrating deterministic forecasts of rare events. *Wea. Forecasting*, **27**, 531-538.

Monteverdi, J. P., C. A. Doswell III, and Gary S. Lipari, 2003: Shear parameter thresholds for forecasting tornadoes in northern and central California. *Wea. Forecasting*, **18**, 357-370.

Rasmussen, E. N., 2003: Refined supercell and tornado forecast parameters. *Wea. Forecasting*, **18**, 530-535.

_____, and D. O. Blanchard, 1998: A baseline climatology of sounding-derived supercell and tornado forecast parameters. *Wea. Forecasting*, **13**, 1148–1164.

Schneider, R. S., and A. R. Dean, 2008: A comprehensive 5-year severe storm environment climatology for the continental United States. Preprints, *24th Conf. Severe Local Storms*, Savannah GA., Amer. Meteor. Soc., 16A.4.

Smith, B. T., R. L. Thompson, J. S. Grams, C. Broyles, and H. E. Brooks, 2012: Convective modes for significant severe thunderstorms in the contiguous United States. Part I: Storm classification and climatology. *Wea. Forecasting*, **27**, 1114-1135.

Sobash, R. A., J. S. Kain, D. R. Bright, A. R. Dean, M. C. Coniglio, and S. J. Weiss, 2011: Probabilistic forecast guidance for severe thunderstorms based on the identification of extreme phenomena in convection-allowing model forecasts. *Wea. Forecasting*, **26**, 714–728.

Thompson, R. L., B. T. Smith, J. S. Grams, A. R. Dean, and C. Broyles, 2012: Convective modes for significant severe thunderstorms in the contiguous United States. Part II: Supercell and QLCS tornado environments. *Wea. Forecasting*, **27**, 1136-1154.

_____, C. M. Mead, and R. Edwards, 2007: Effective storm-relative helicity and bulk shear in supercell thunderstorm environments. *Wea. Forecasting*, **22**, 102-115.

_____, R. Edwards, J. A. Hart, K. L. Elmore, and P. Markowski, 2003: Close proximity soundings within supercell environments obtained from the Rapid Update Cycle., *Wea. Forecasting*, **18**, 1243–1261.

_____, J. M. Lewis, and R. A. Maddox, 1994: Autumnal return of tropical air to the Gulf of Mexico's coastal plain. *Wea. Forecasting*, **9**, 348-360.

Trapp, R. J., S. A. Tessendorf, E. S. Godfrey, and H. E. Brooks, 2005: Tornadoes from squall lines and bow echoes: Part I: Climatological distribution. *Wea. Forecasting*, **20**, 23-34.

Wakimoto, R. M., and J. Wilson, 1989: Nonsupercell tornadoes. *Mon. Wea. Rev*., **117**, 1118-1140.

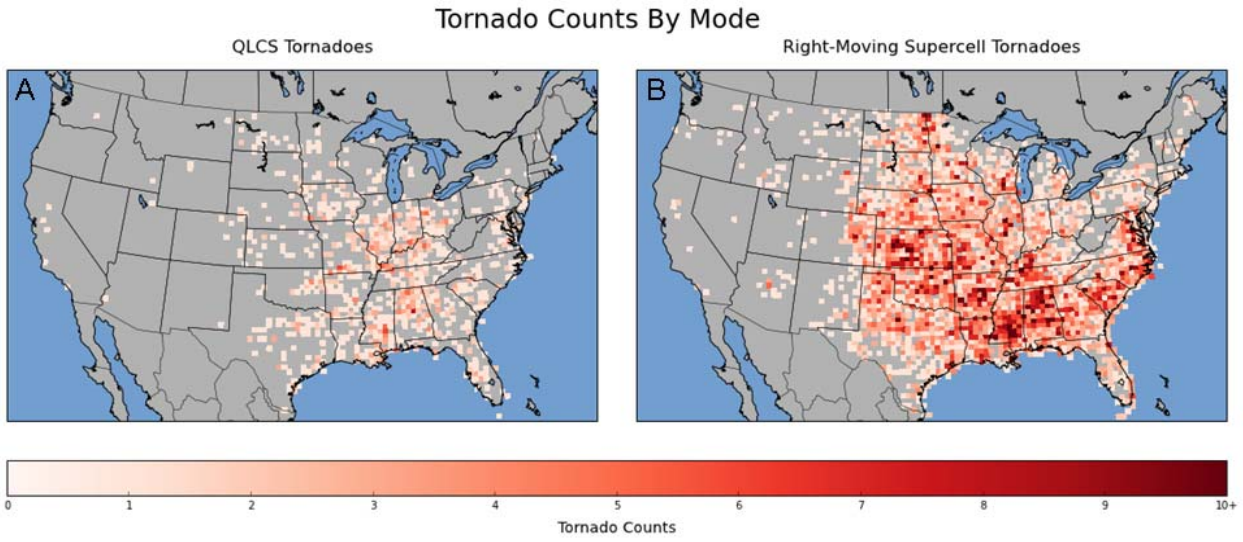

Figure 1. Raw grid-hour counts for a) 1168 QLCS tornadoes and b) 7669 right-moving supercell tornadoes from the Thompson et al. (2012) sample spanning 2003-2011. Peak grid-hour counts are 8 and 17 for QLCS and right-moving supercell tornadoes, respectively.

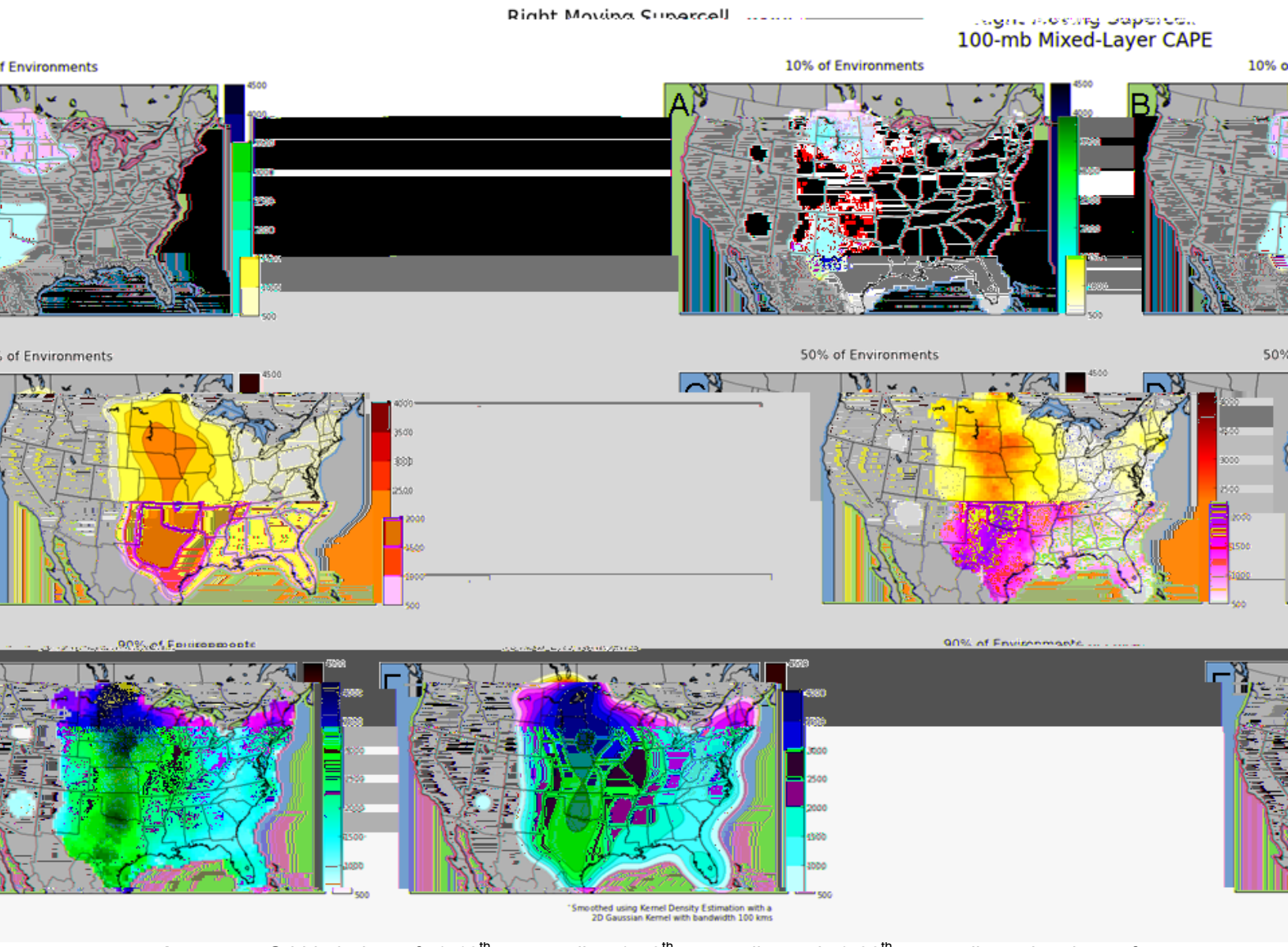

Figure 2. Gridded plots of a) 10th percentile, c) 50th percentile, and e) 90th percentile rank values of MLCAPE (J kg^{-1}) associated with tornadic right-moving supercells from the T12 sample. The gridded plots represent the accumulated distribution of all events within a 120 km radius of each grid box. A kernel density smoother with 100 km radius of influence is applied to the 10th, 50th, and 90th percentile values in b), d), and f), respectively.

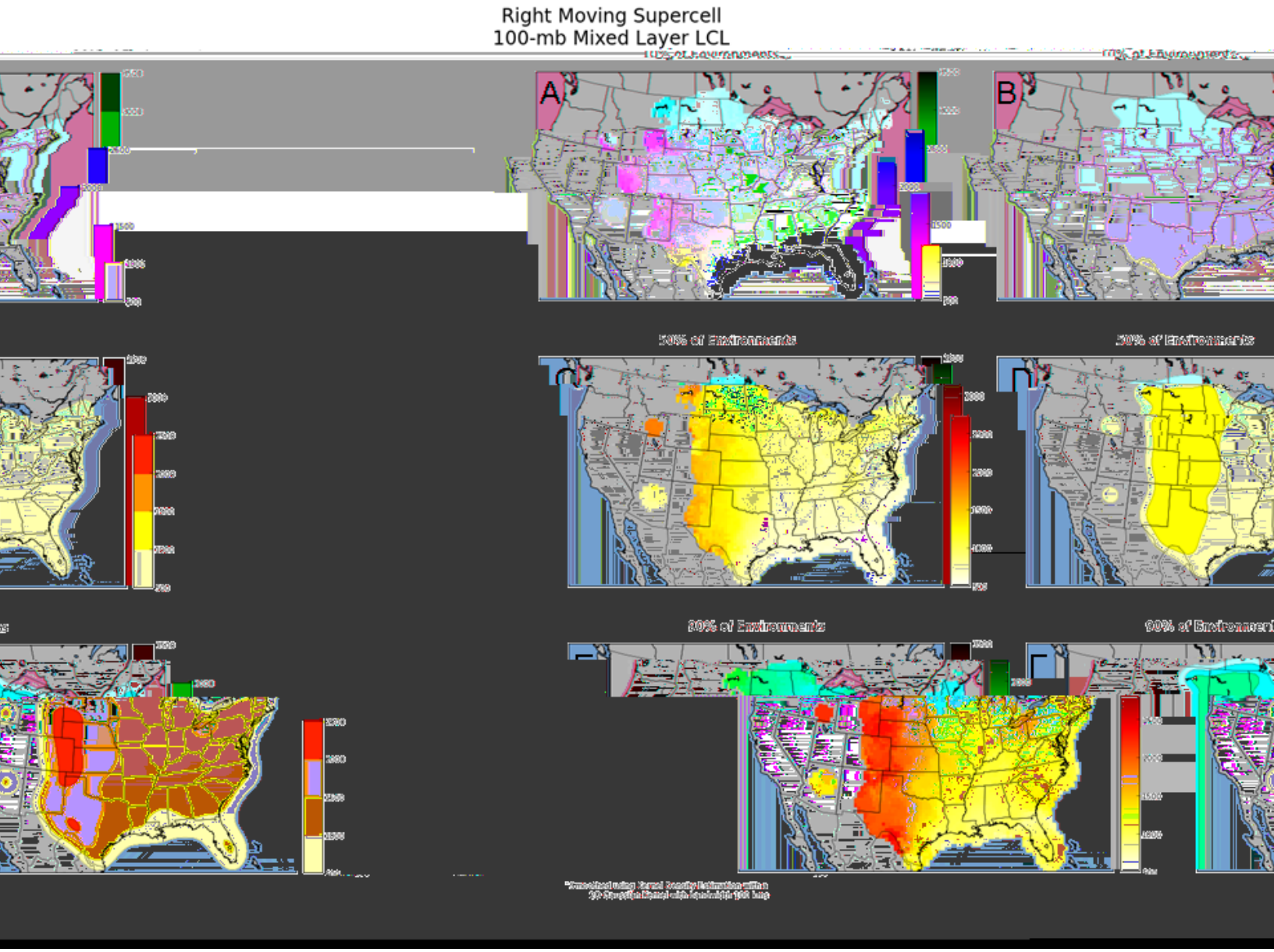

Figure 3. Same as Fig. 2, except for MLLCL height (m AGL).

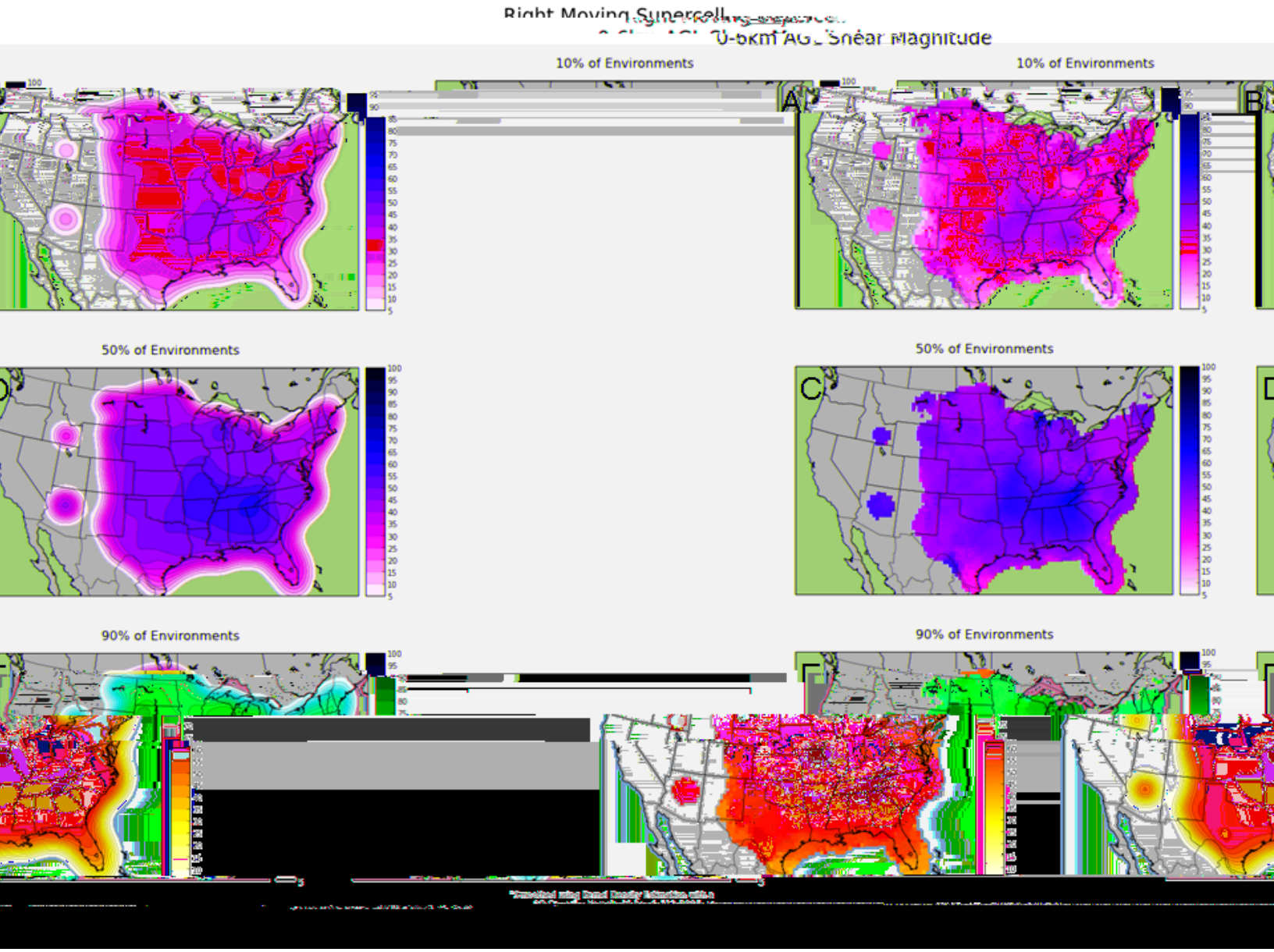

Figure 4. Same as Fig. 2, except for 0–6-km BWD (kt).

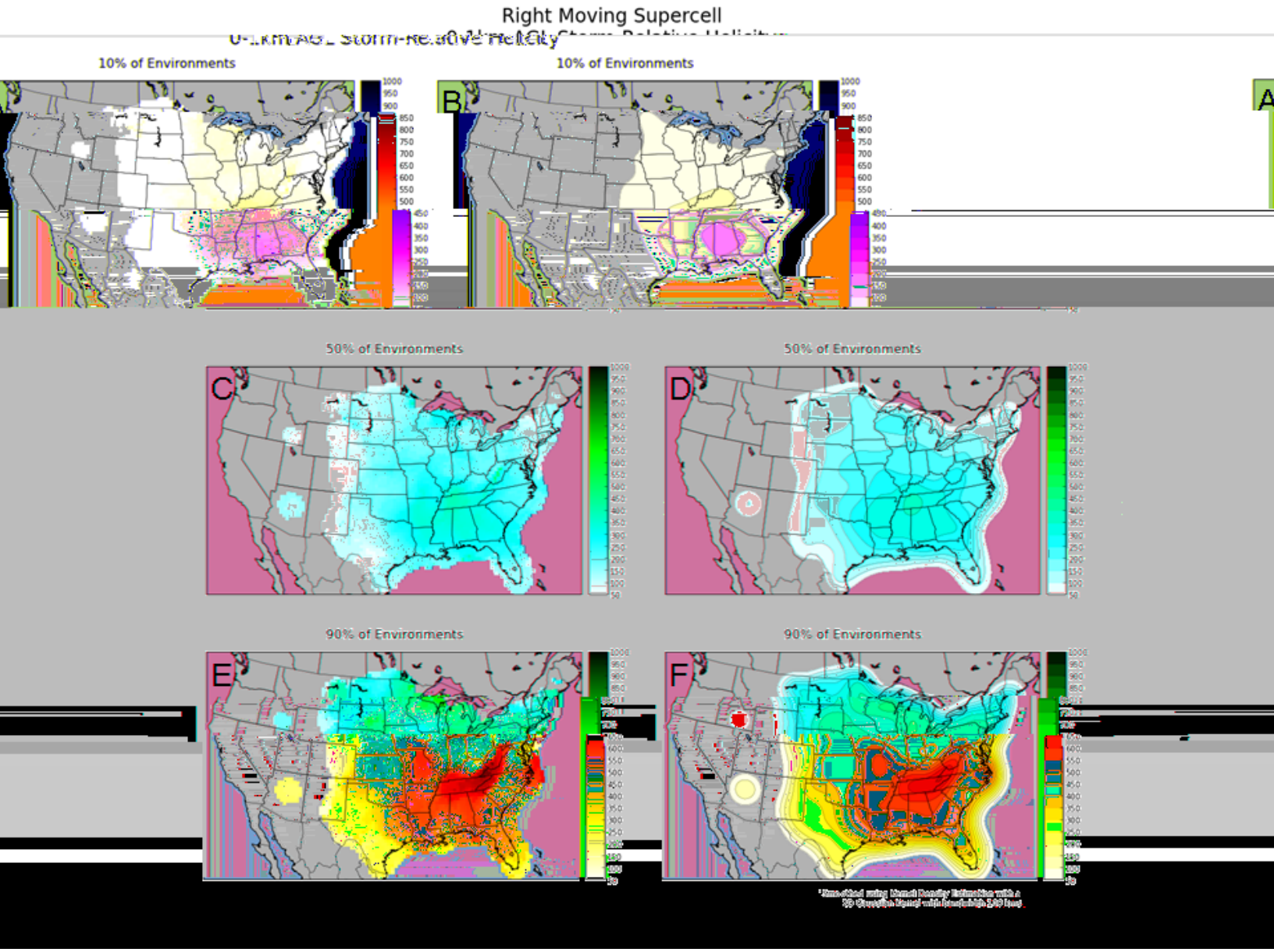

Figure 5. Same as Fig. 2, except for 0–1-km SRH (m^2 s^{-2}).

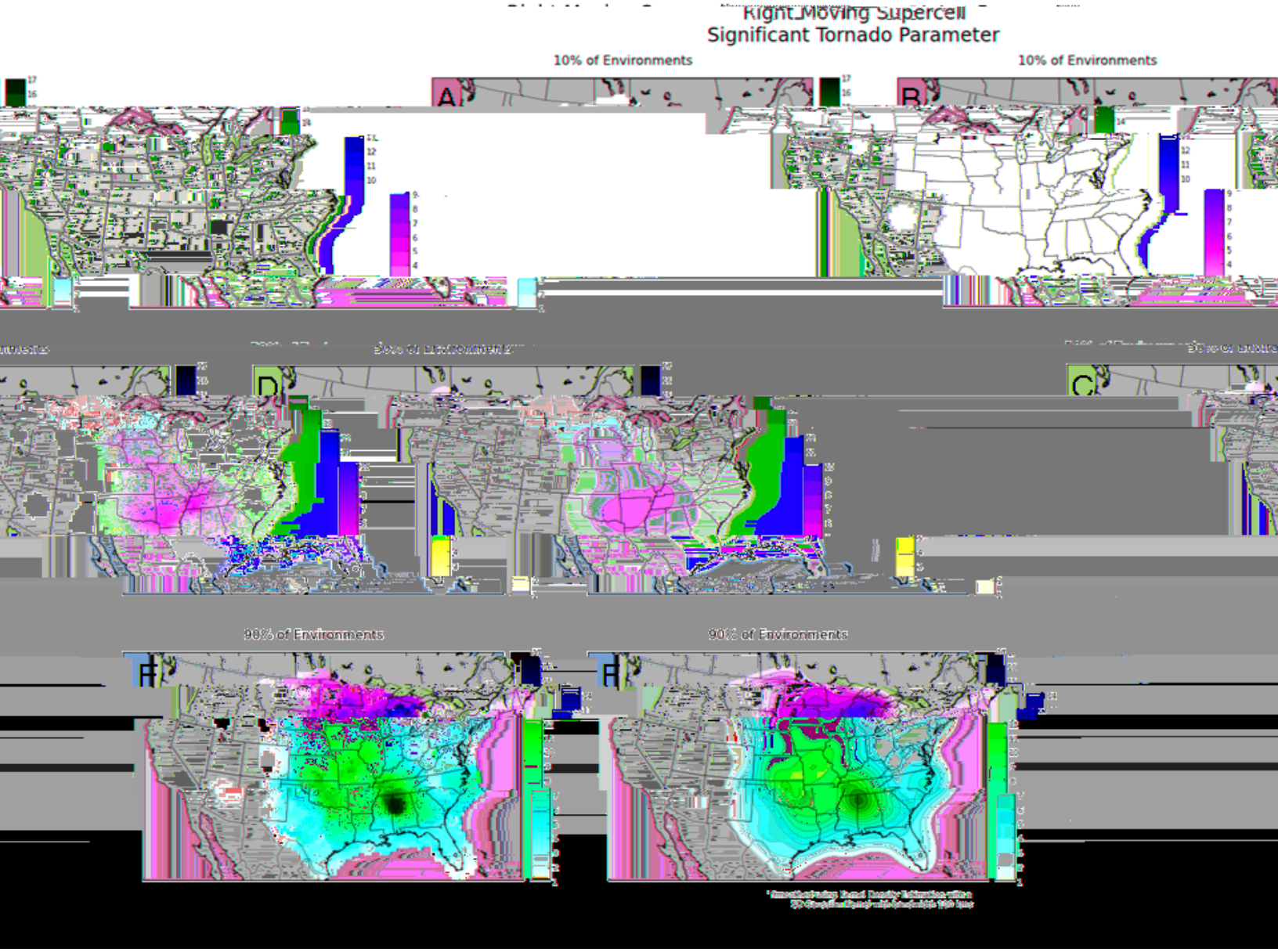

Figure 6. Same as Fig. 2, except for STP (dimensionless).

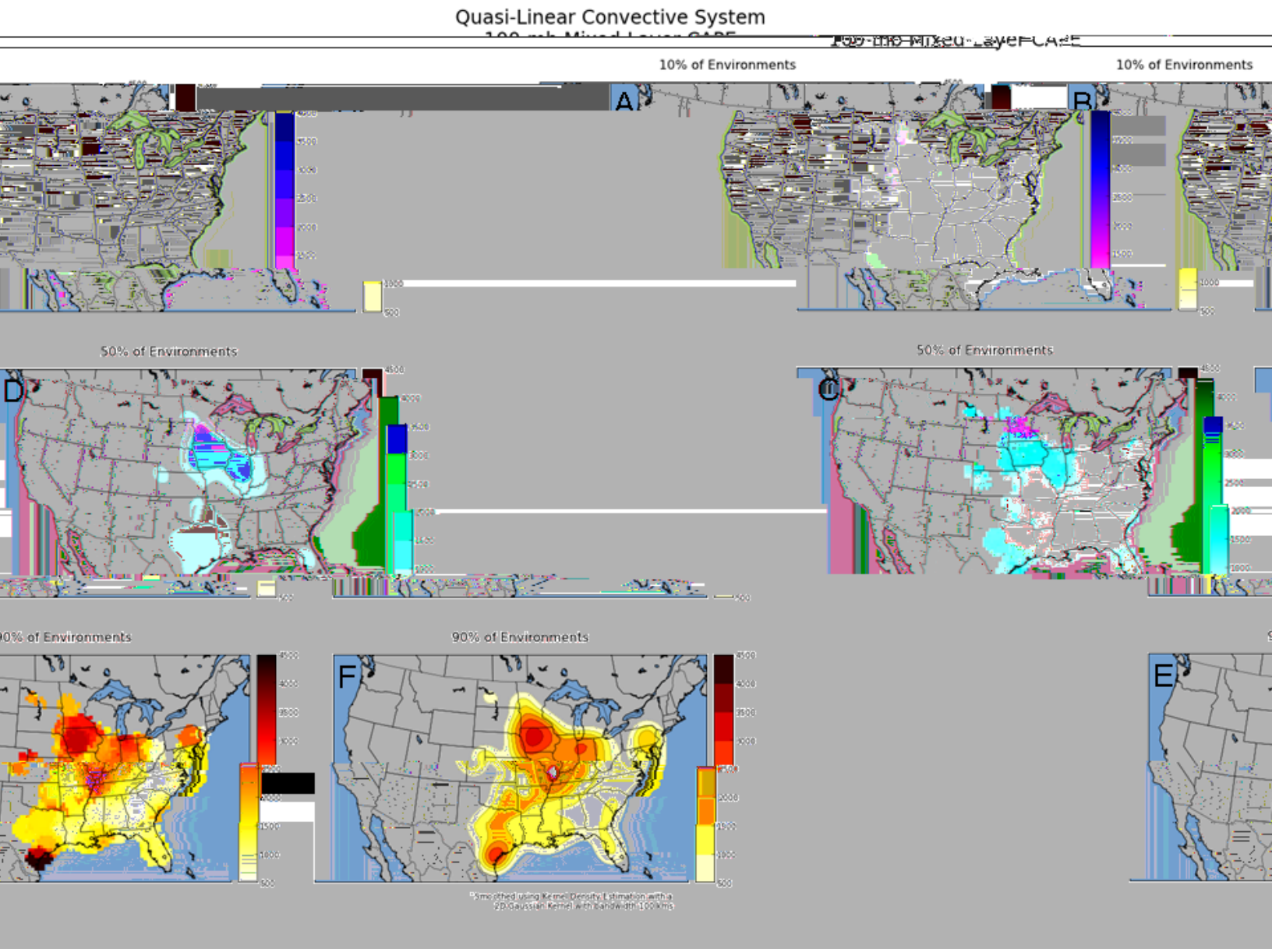

Figure 7. Same as Fig. 2, except for MLCAPE (J kg^{-1}) associated with QLCS tornadoes.

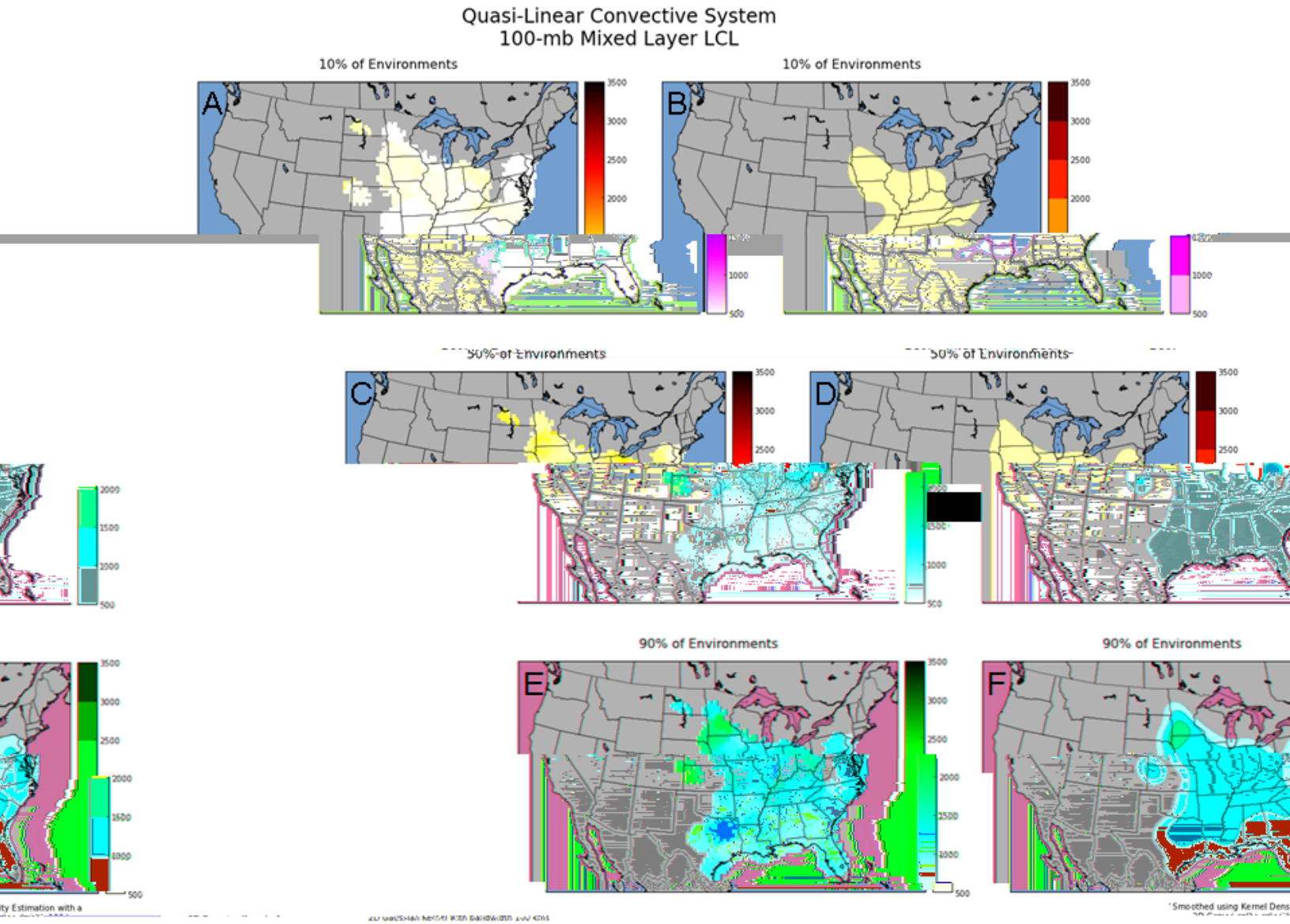

Figure 8. Same as Fig. 3, except for MLLCL height (m AGL) associated with QLCS tornadoes.

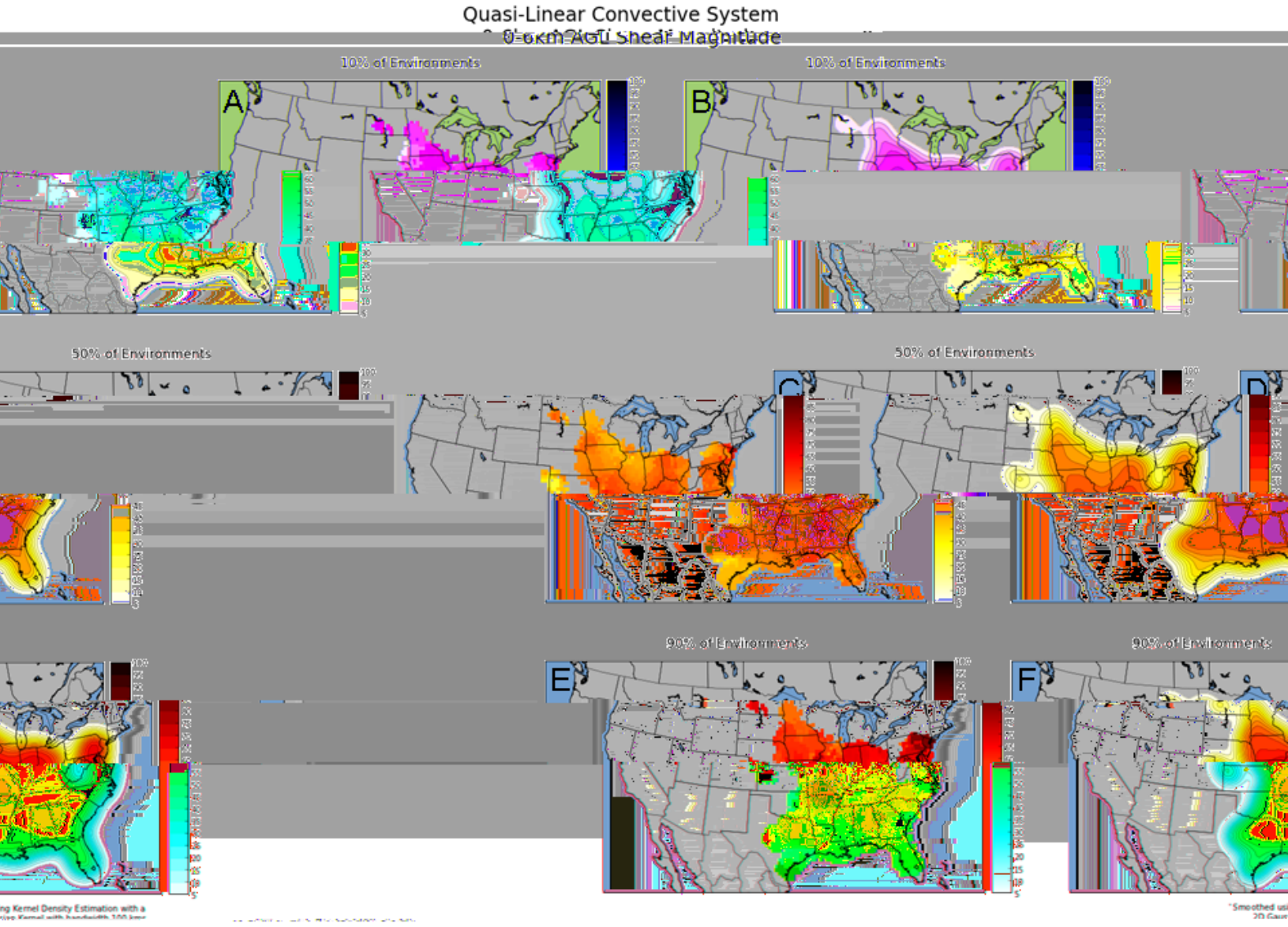

Figure 9. Same as Fig. 4, except for 0–6-km BWD (kt) associated with QLCS tornadoes.

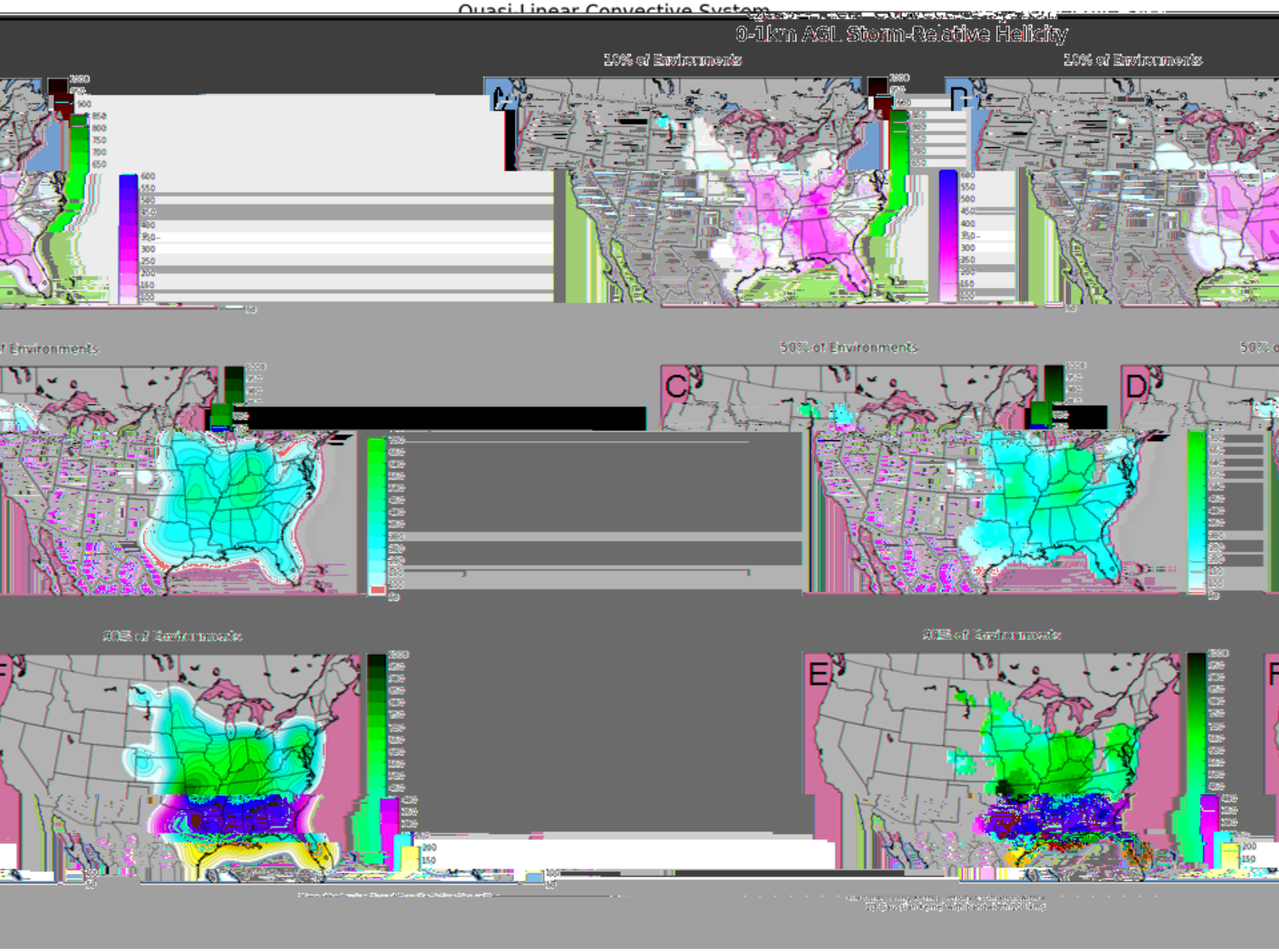

Figure 10. Same as Fig. 5, except for 0–1-km SRH (m^2 s^{-2}) associated with QLCS tornadoes.

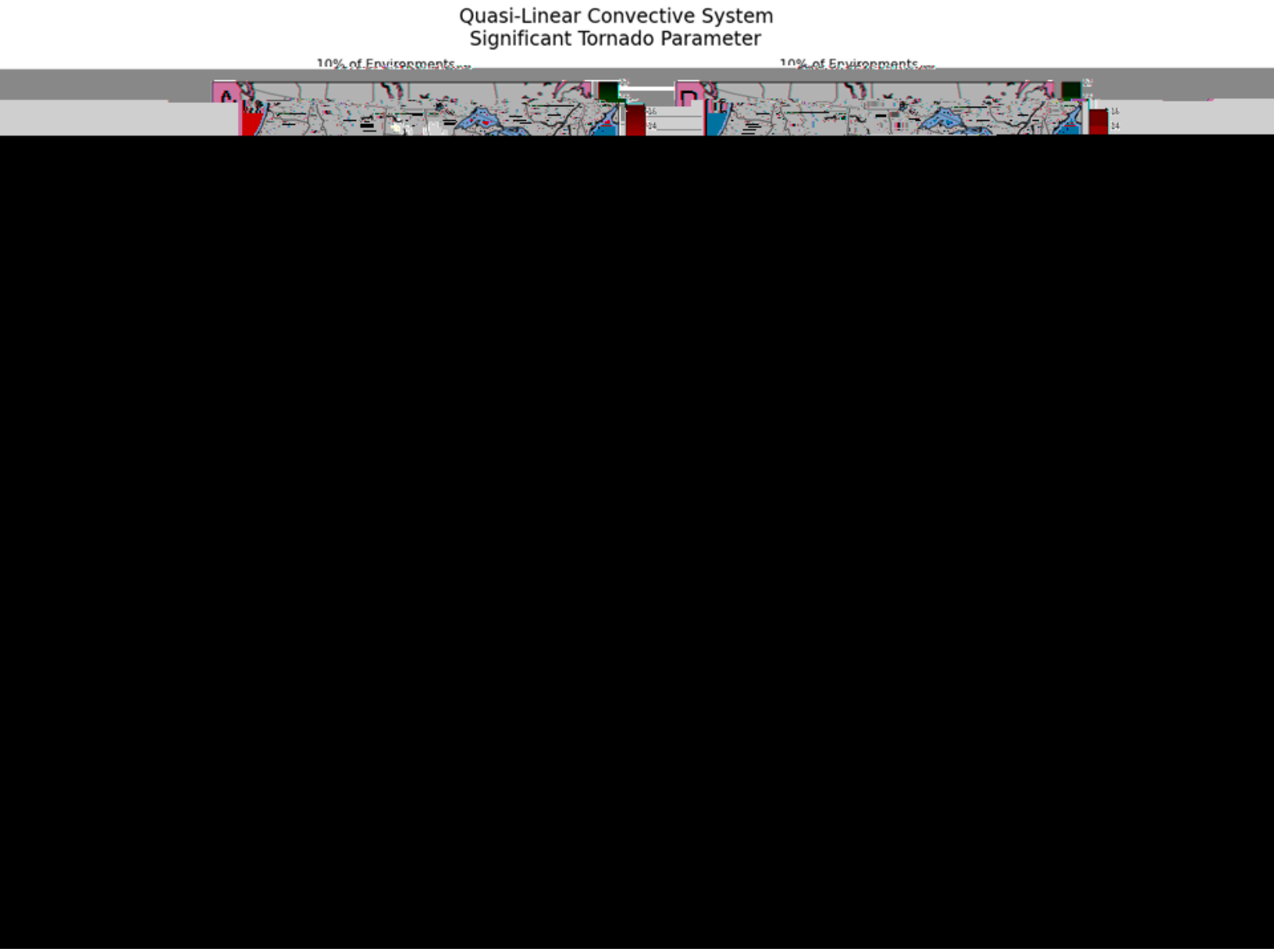

Figure 11. Same as Fig. 6, except for STP (dimensionless) associated with QLCS tornadoes.

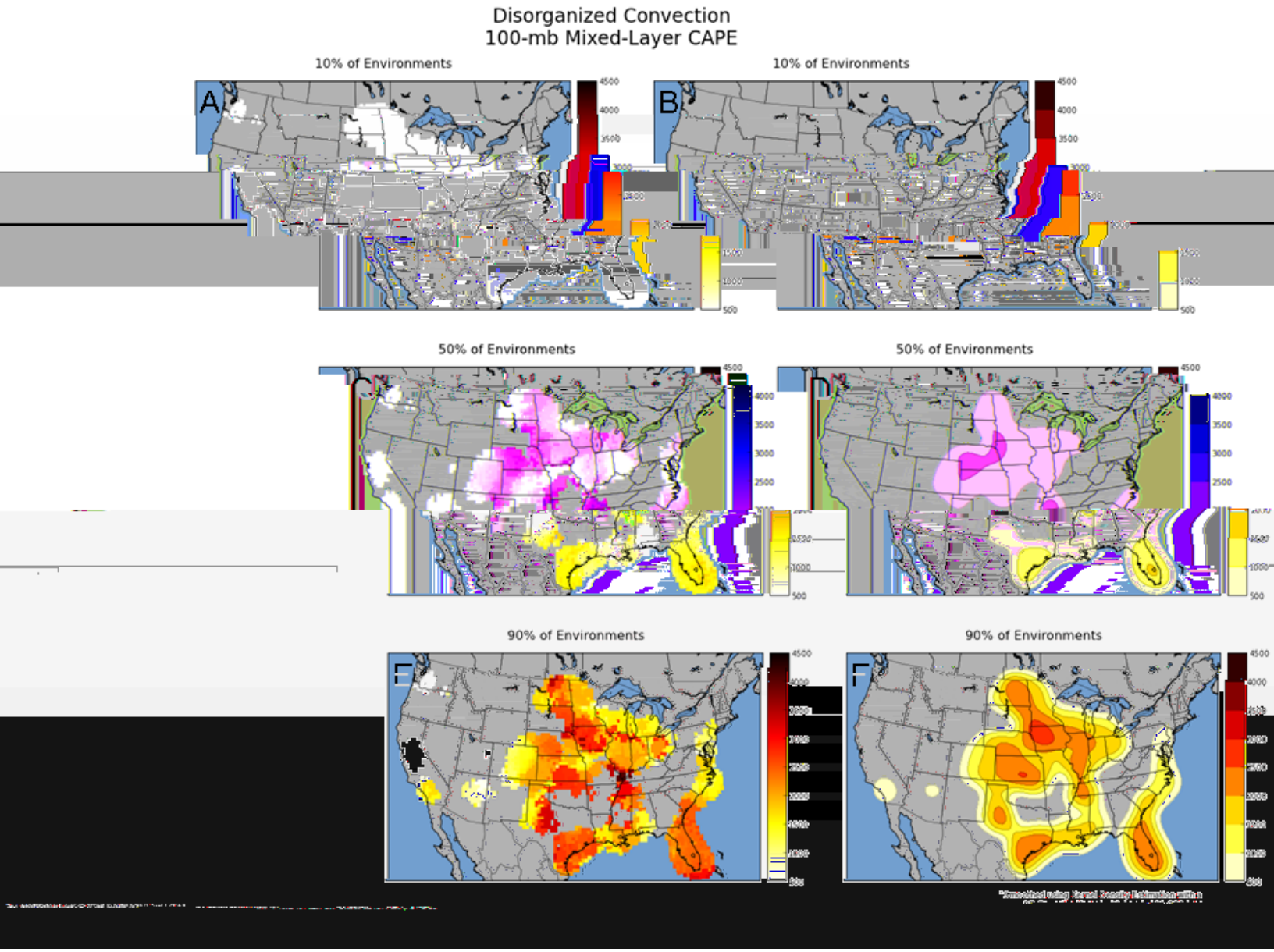

Figure 12. Same as Fig. 2, except for MLCAPE (J kg^{-1}) associated with disorganized tornadic storms.

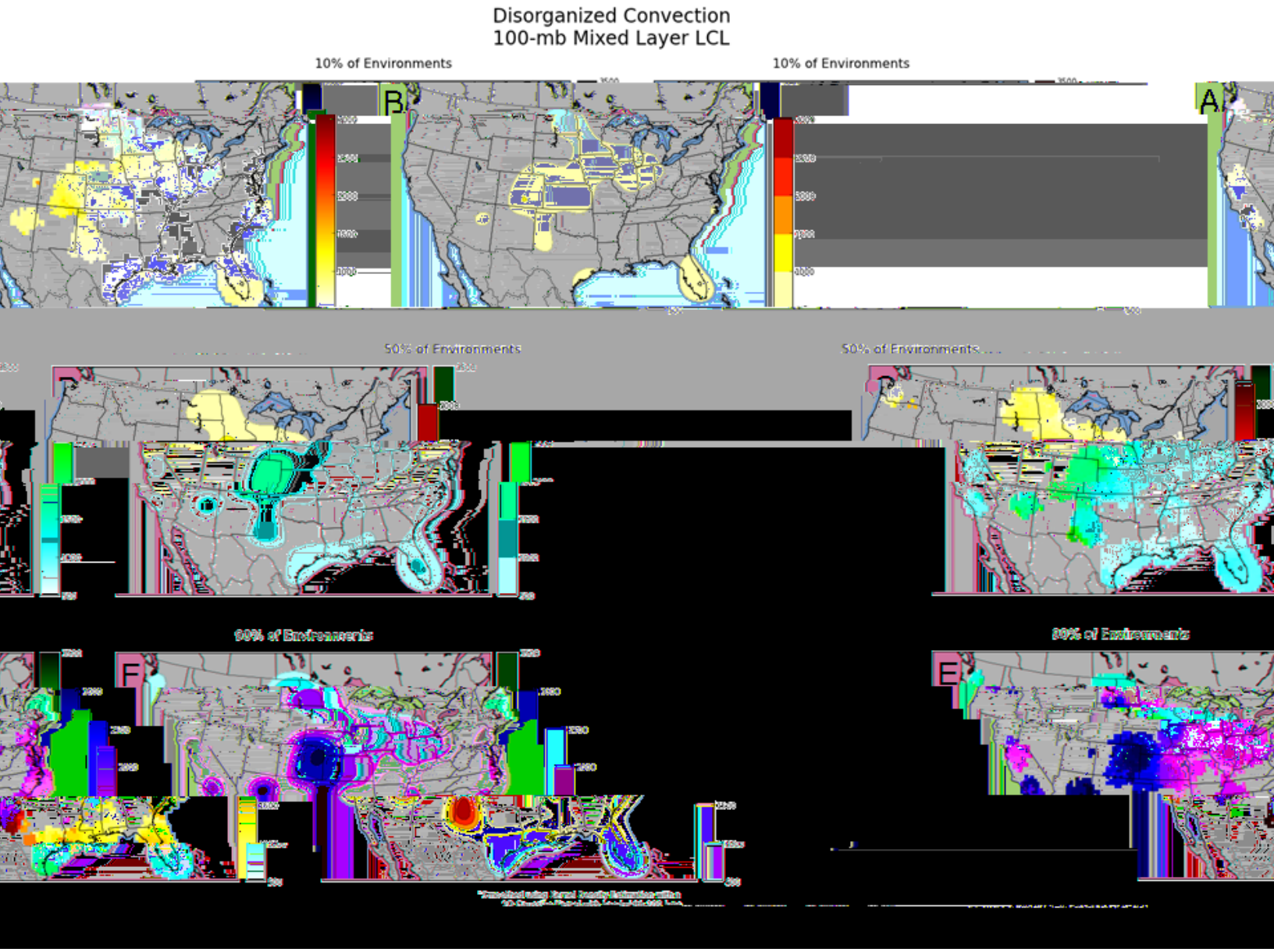

Figure 13. Same as Fig. 3, except for MLLCL (m AGL) associated with disorganized tornadic storms.

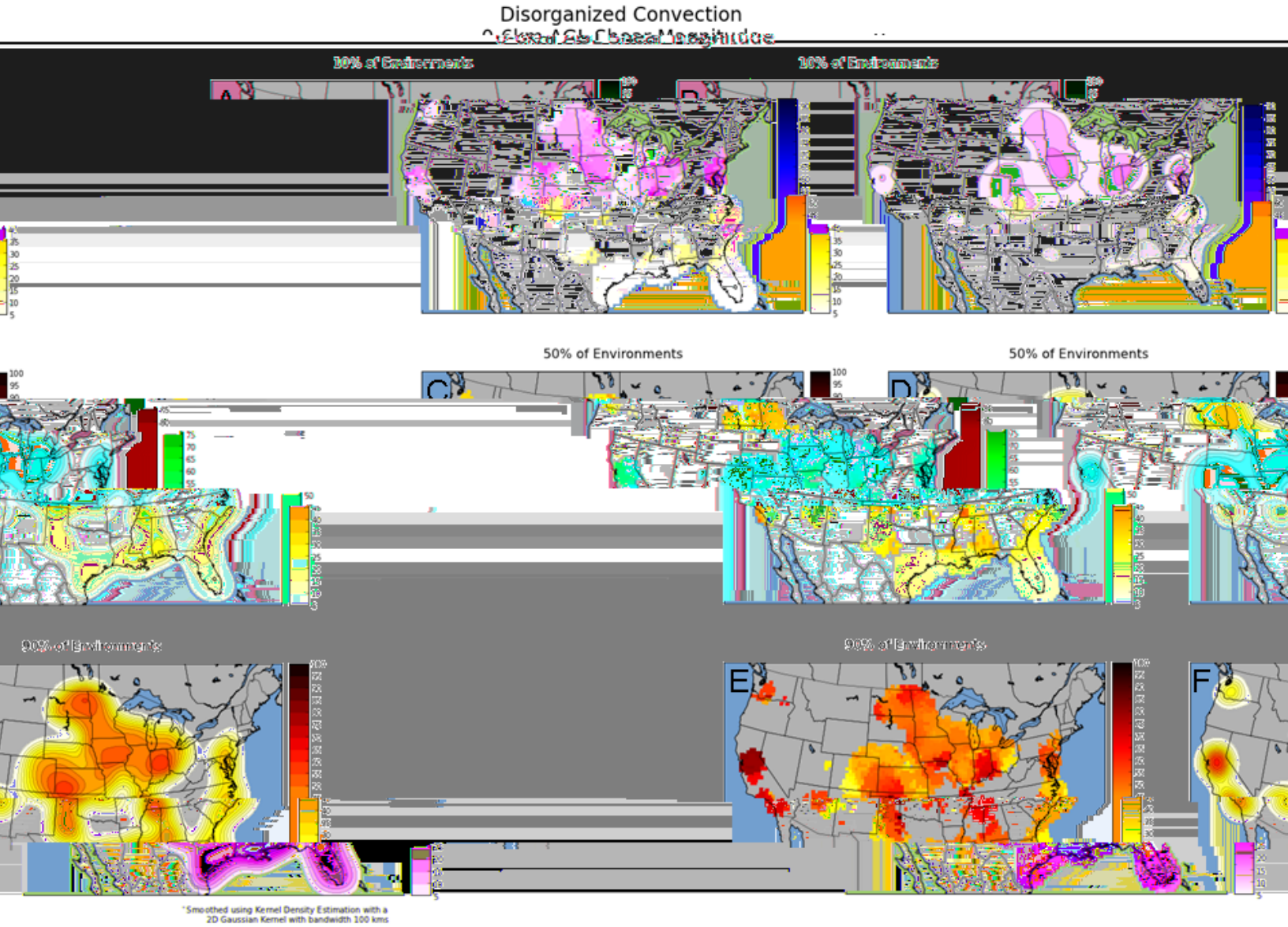

Figure 14. Same as Fig. 4, except for 0–6-km BWD (kt) associated with disorganized tornadic storms.

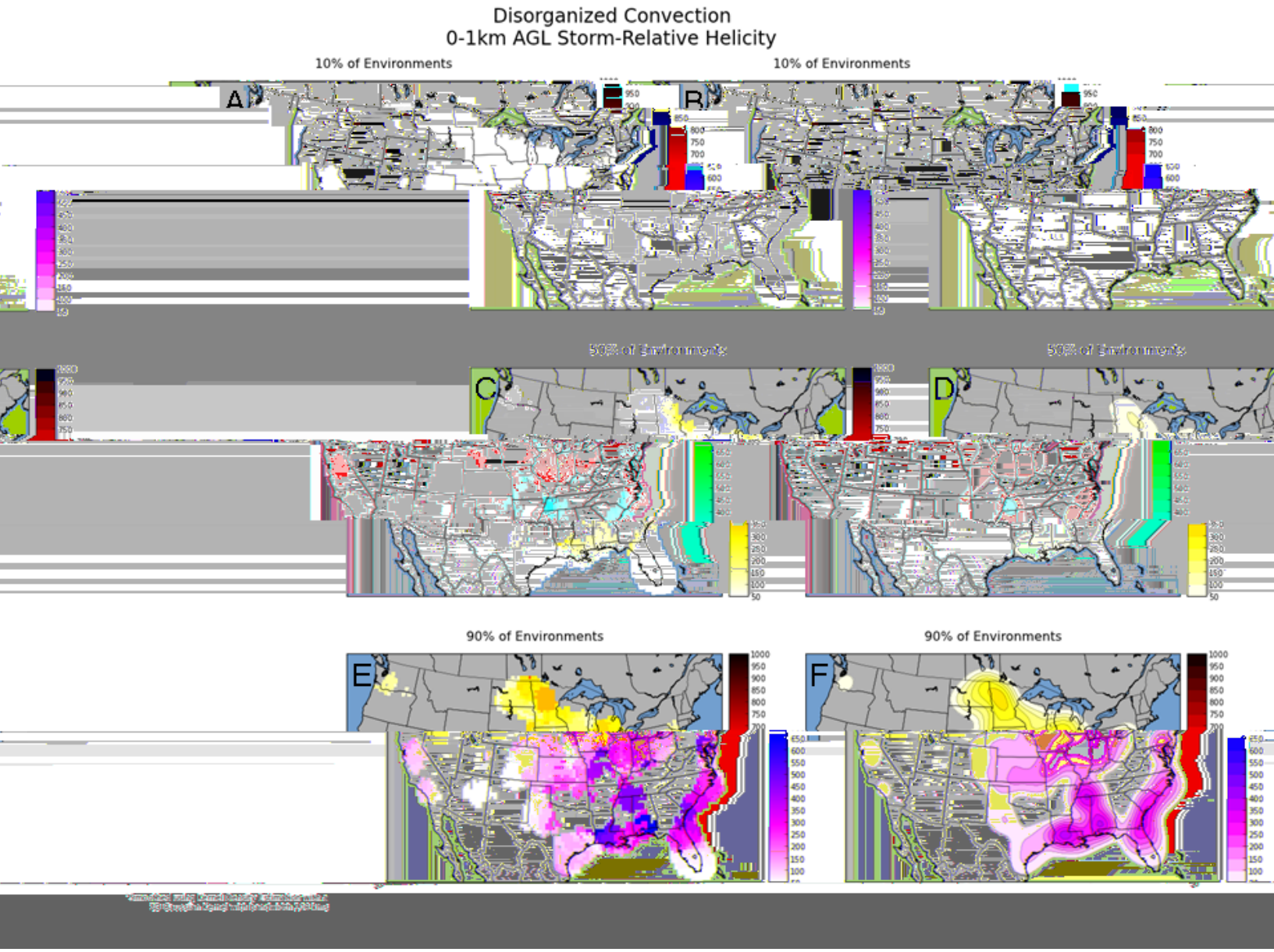

Figure 15. Same as Fig. 5, except for 0–1-km SRH (m^2 s^{-2}) associated with disorganized tornadic storms.

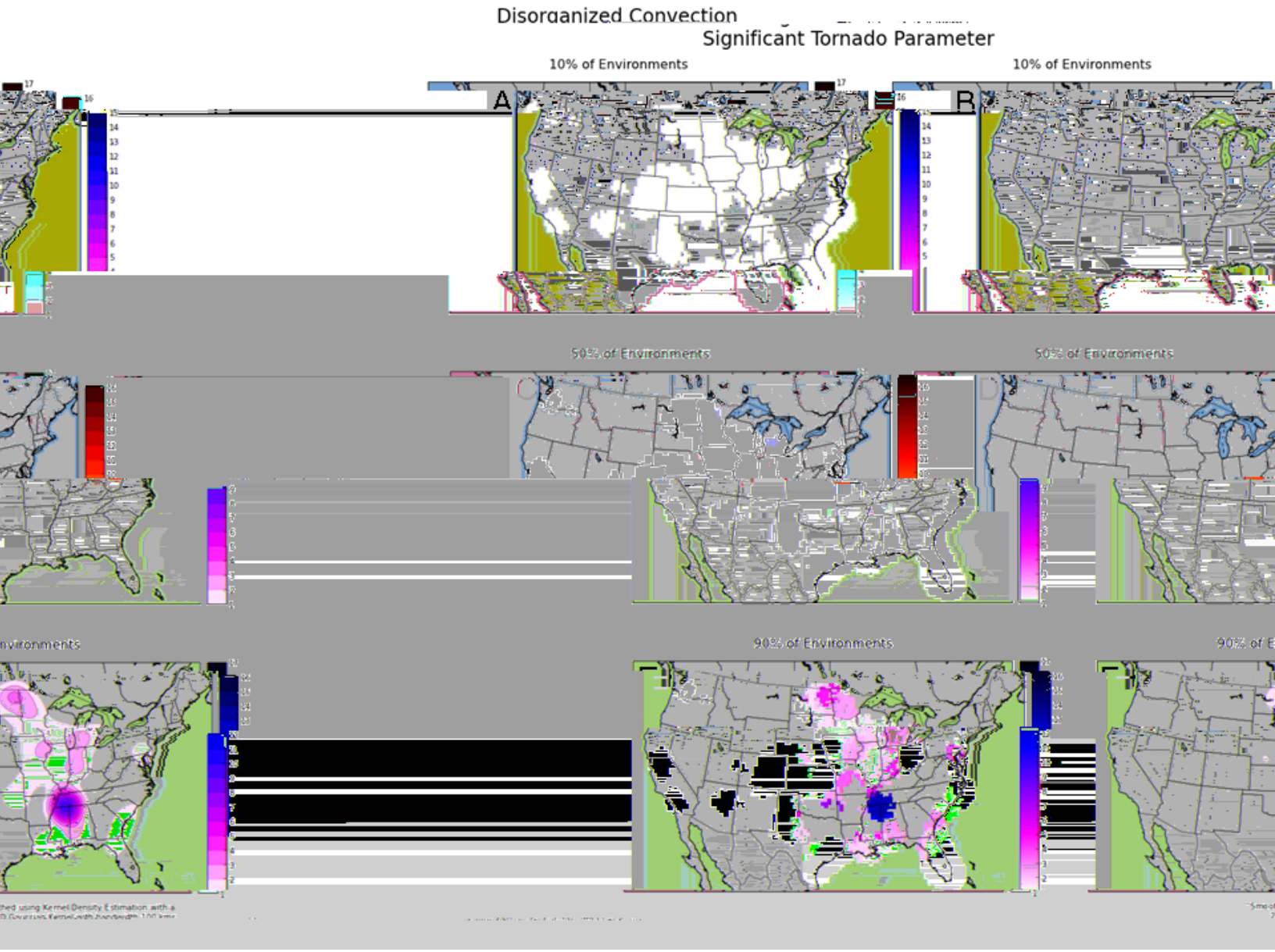

Figure 16. Same as Fig. 6, except for STP (dimensionless) associated with disorganized tornadic storms.